Research Article

Dong Yawei, Zhang Yang, and Yan Jianwei*

# Exact solutions of bending deflection for single-walled BNNTs based on the classical Euler–Bernoulli beam theory

https://doi.org/10.1515/ntrev-2020-0075
received September 13, 2020; accepted September 23, 2020

**Abstract:** At the nanolevel, a classical continuum approach seems to be inapplicable to evaluate the mechanical behaviors of materials. With the introduction of scale parameter, the scale effect can be reasonably described by the modified continuum theory. For boron nitride nanotubes (BNNTs), the scale effect can be reflected by the curvature and the dangling bonds at both ends, mainly the former for a slender tube. This study aims to achieve a good capability of classical Euler–Bernoulli theory to directly predict the bending behaviors of single-walled BNNTs without introducing scale parameters. Elastic properties of BNNTs involving the scale effect have been first conducted by using an atomistic-continuum multiscale approach, which is directly constructed based on the atomic force field. The well-determined hexagonal boron nitride sheet is inherited in the present study of single-walled BNNTs which can be viewed as rolling up a boron nitride sheet into a seamless hollow cylinder. Euler–Bernoulli theory solution of bending deflection on the basis of the present thickness is found to be much closer to the atomistic-continuum simulation results than the commonly used interlayer space. Case studies with different tubular lengths, radii and constraints are investigated, and from which the yielded scattered scale parameters in modified continuum theories are discussed.

* **Corresponding author: Yan Jianwei,** School of Civil Engineering and Architecture, East China Jiaotong University, Nanchang, Jiangxi, 330013, People's Republic of China; National Experimental Teaching Demonstration Center of Civil Engineering, East China Jiaotong University, Nanchang, Jiangxi, 330013, People's Republic of China, e-mail: tyanjianwei@jnu.edu.cn
**Dong Yawei:** School of Science, Nanjing University of Science and Technology, Nanjing, Jiangsu, 210094, People's Republic of China
**Zhang Yang:** School of Science, Nanjing University of Science and Technology, Nanjing, Jiangsu, 210094, People's Republic of China; Department of Architecture and Civil Engineering, City University of Hong Kong, Kowloon, Hong Kong, 999077, People's Republic of China

**Keywords:** Euler–Bernoulli beam model, boron nitride nanotube, bending deflection, material thickness, scale effect

## 1 Introduction

As a landmark one-dimensional material, carbon nanotubes (CNTs) have attracted huge interest of research community because they possess outstanding electronic homogeneity, high strength and low density [1–5]. These excellent properties make CNTs widely applied in engineering, especially those related to electrical industry such as sensors and flexible electronics [6–13]. Several years later after the synthesis of CNTs, Blasé et al. [14] theoretically predicted the possibility and superior characteristic of boron nitride nanotubes (BNNTs) that alternately replaced the carbon atoms of CNTs by boron and nitrogen atoms. Similarly, BNNTs can also be viewed as rolling up boron nitride sheets along different directions, which yields zigzag, armchair and chiral BNNTs. Nevertheless, as pointed out by Blasé et al. [14], BNNTs are constant-band-gap materials, independent of their radius and helicity. BNNTs also possess other properties superior to CNTs such as structural stability [15–17], high mechanical strength [18–23] and heat conduction [24–26], thus being promising for various engineering applications. In addition, the nature that BNNTs do not absorb visible and infrared light [27] is helpful to protect biological materials from overheating and decomposition [28,29]. Although their biocompatibility still needs further experiment assessments, many researchers have devoted themselves to investigate their application in nanosensor devices according to the frequency shift or conductance change [30–32].

It is essential to well understand the mechanical behaviors of BNNTs before their application. Experimental investigations, analytical solutions and numerical simulations regarding the mechanical performance of BNNTs have been continuously conducted. At the nanolevel,

experimental study on the mechanical behaviors of BNNTs is a severe challenge due to the difficulties related to the handling and controlling of monoatomic thickness and manipulating of extremely low force for load imposition. Therefore, appropriate non-experimental methods were sought to construct for BNNT investigations. Microlevel methods such as quantum mechanics and molecular dynamics [33–35] are capable of tracing atomic displacements but computationally expensive, and thus it is difficult to fulfill the engineering requirement. Classical continuum theory can easily solve the huge cost problems. Nevertheless, the constructed constitutive equations are questionable when applying in the field of nanomechanics owing to the microscale effect and discrete structure. That is to say, the fact that material properties are size-dependent must be considered, which requires an extra modification of traditional constitutive equations to consider the scale effect. Many modified theories are proposed to consider the small-scale effect such as strain gradient theory [36–38] and nonlocal elasticity theory [39–41]. Even though these modified theories have made many significant achievements to well match with the atomic simulations, the external introduced scale parameters and the bending rigidity were found to be dependent on boundary conditions, chirality, mode shapes, number of walls and the nature of motions. In other words, for different specific case studies, the scale parameter as well as bending rigidity should be re-calibrated and scattered. In a physical sense, the scale parameter is only material-dependent which should be well-determined. Thus, the aforementioned parameter re-calibrated procedure only has mathematical meaning. Why do so many scattered parameters exist? One of the most important reasons is that untrue thickness values and thus moment of inertia are employed such as the widely used interlayer space of multi-layer boron nitride sheets.

In our previous work, the caused errors on studying the natural frequencies of hexagonal boron nitride (h-BN) sheet by the classical plate theory when employing the interlayer space and other values as the material thickness in comparison with full atomic simulations have been studied in detail. To overcome this issue, we employed a "bottom-up" atomistic-continuum approach which is on the basis of force field to avoid introducing any elastic parameters and used a homogenization technique to eliminate the influence of dangling bonds. By fitting the results obtained by the classical plate theory, the one-atomic material thickness was exactly determined. Such a process has a definite physical meaning without confusing readers. As a result, we exactly extracted it to be 0.0906 nm by fitting the numerically calculated fundamental frequencies as well as higher-order ones of a series of simply supported h-BN sheets with analytical solutions of the classical plate theory [42].

As discussed, the well-determined one-atomic material thickness is physically accepted. Thus, in this study, we aim to extend our theoretical model to investigate the deformation such as bending deflections of BNNTs in order to further demonstrate the universality. We decouple the material thickness and scale effect on elastic property, which are semi-analytically evaluated by an atomistic-continuum multiscale approach. Then the classical Euler–Bernoulli beam theory (EBT) is employed to investigate the bending deflection behavior of BNNTs. The atomistic-continuum multiscale simulation results for various single-walled BNNTs are also provided for validation.

# 2 Differential equation for bending deflection of BNNTs

## 2.1 EBT

The bending control differential equation for the Euler–Bernoulli beam model can be expressed by:

$$\frac{\mathrm{d}^2 w}{\mathrm{d}x^2} = -\frac{M(x)}{EI(x)}, \tag{1}$$

where $w$ is the bending deflection at $x$ coordinate, $M(x)$ is the bending moment, $E$ is the axial Young's modulus and $I(x)$ is the moment of inertia.

**Case 1.** Simply supported beam

The simply supported boundary conditions are as follows:

$$\begin{cases} x = 0: \quad w(0) = 0, \quad \left.\dfrac{\mathrm{d}^2 w}{\mathrm{d}x^2}\right|_{(0)} = 0 \\ x = l: \quad w(l) = 0, \quad \left.\dfrac{\mathrm{d}^2 w}{\mathrm{d}x^2}\right|_{(l)} = 0. \end{cases} \tag{2}$$

Therefore, the bending deflection for a simply supported beam when imposing a concentrated force at the middle can be obtained by:

$$w_{\mathrm{sf}}(x) = \frac{F_{\mathrm{p}} x\left(\frac{3}{4}l^2 - x^2\right)}{12EI}, \tag{3}$$

where $F_p$ is a concentrated force imposed at the one-dimensional beam model under EBT, with the midpoint bending deflection being:

$$w_{sf}(l/2) = \frac{F_p l^3}{48EI}. \tag{4}$$

When imposing uniformly distributed load $q$ at the beam, the midpoint bending deflection is solved by:

$$w_{sq}(l/2) = \frac{5ql^4}{384EI}. \tag{5}$$

**Case 2.** Clamped beam

The clamped boundary conditions are as follows:

$$\begin{cases} x = 0: \quad w(0) = 0, \quad \left.\dfrac{dw}{dx}\right|_{(0)} = 0 \\ x = l: \quad w(l) = 0, \quad \left.\dfrac{dw}{dx}\right|_{(l)} = 0. \end{cases} \tag{6}$$

The maximum bending deflection occurs at the midpoint of the beam when imposing a concentrated force at the middle. Substituting the boundary condition of equation (6) into the differential equation (1) to determine the integration coefficient, the midpoint bending deflection for a clamped beam can be solved by:

$$w_{cf}(l/2) = \frac{F_p l^3}{192EI}. \tag{7}$$

When imposing uniformly distributed load at the beam, it becomes:

$$w_{cq}(l/2) = \frac{ql^4}{384EI}. \tag{8}$$

## 2.2 Atomistic-continuum multiscale approach

Atomistic-continuum multiscale approach is also provided for numerical simulation of the bending behaviors of BNNTs. Our recently developed atomistic-continuum multiscale approach is constructed by using the higher-order Cauchy–Born rule to provide a refined linkage between the deformation of lattice structure and the macroscale continuum deformation gradient field [42–44], which can be expressed by:

$$\mathbf{r}_{IJ} = \mathbf{F} \cdot (\mathbf{R}_{IJ} + \boldsymbol{\eta}) + \frac{1}{2}\mathbf{G} : [(\mathbf{R}_{IJ} + \boldsymbol{\eta}) \otimes (\mathbf{R}_{IJ} + \boldsymbol{\eta})], \tag{9}$$

where $\mathbf{r}_{IJ}$ is the deformed bond vector in the current configuration, $\mathbf{R}_{IJ}$ denotes the initial bond vector in the reference configuration and $\boldsymbol{\eta}$ is the inner shift.

As detailed in our work [45], the hollow seamless cylindrical shell structure of single-walled BNNTs can be viewed as rolling the equilibrium h-BN sheet with three geometrical parameters $\lambda_1$, $\lambda_2$ and $\theta$, respectively. The deformation process can be expressed by:

$$\begin{cases} x_1 = X_1\lambda_1 \cos\theta \\ x_2 = \dfrac{\Gamma\lambda_2}{2\pi} \sin\left[2\pi\left(\dfrac{X_2}{\Gamma} + \dfrac{X_1\lambda_1 \sin\theta}{\Gamma\lambda_2}\right)\right] \\ x_3 = \dfrac{\Gamma\lambda_2}{2\pi} - \dfrac{\Gamma\lambda_2}{2\pi} \cos\left[2\pi\left(\dfrac{X_2}{\Gamma} + \dfrac{X_1\lambda_1 \sin\theta}{\Gamma\lambda_2}\right)\right], \end{cases} \tag{10}$$

where $\boldsymbol{x} = \boldsymbol{x}(x_1, x_2, x_3)$ and $\boldsymbol{X} = \boldsymbol{X}(X_1, X_2)$ are the current and reference configurations. These three geometrical parameters can be determined by minimizing the strain energy of BNNTs to seek the equilibrium configuration. Tersoff–Brenner empirical potential is adopted to reflect the atomic force field:

$$V_B(r_{IJ}) = V_R(r_{IJ}) - B_{IJ} V_A(r_{IJ}), \tag{11}$$

where $r_{IJ}$ and $B_{IJ}$ denote the bond length and a multi-body coupling between atoms I and J, respectively. It can be directly obtained from equation (11) that the energy of atom $I$ is a function of bonds connecting it to neighboring three atoms:

$$W(\boldsymbol{F}, \boldsymbol{G}) = \frac{1}{2}\sum_{J=1}^{3} V_{IJ}(r_{I2}, r_{I2}, r_{I3}) = V_I[\boldsymbol{F}, \boldsymbol{G}, \boldsymbol{\eta}]. \tag{12}$$

In a specific deformation system, the partial derivative strain energy $V_I$ with respect to the inner shift vector $\boldsymbol{\eta}$ must be zero to ensure the minimum potential of the system:

$$\frac{\partial V_I}{\partial \boldsymbol{\eta}} = 0. \tag{13}$$

Therefore, it is easy to find that the potential only relates to $\boldsymbol{F}$ and $\boldsymbol{G}$:

$$W(\boldsymbol{F}, \boldsymbol{G}) = V_I[\boldsymbol{F}, \boldsymbol{G}, \boldsymbol{\eta}] = V_I[\boldsymbol{F}, \boldsymbol{G}, \boldsymbol{\eta}(\boldsymbol{F}, \boldsymbol{G})]. \tag{14}$$

These three geometrical parameters and inner shift can be finally determined by minimizing the corresponding potential:

$$\frac{\partial V_I}{\partial \lambda_1} = \frac{\partial V_I}{\partial \lambda_2} = \frac{\partial V_I}{\partial \theta} = \frac{\partial V_I}{\partial \eta_1} = \frac{\partial V_I}{\partial \eta_2} = 0. \tag{15}$$

Axial Young's modulus of BNNTs is as follows:

$$E = \frac{\partial^2 v_0}{\partial \lambda_1^2} - \frac{\left(\frac{\partial^2 v_0}{\partial \lambda_1 \partial \lambda_2}\right)^2}{\frac{\partial^2 v_0}{\partial \lambda_2^2}}, \tag{16}$$

where $v_0$ is the strain energy at the nearby initial equilibrium position. Poisson's ratio is calculated by:

$$\mu = \frac{\frac{\partial^2 v_0}{\partial \lambda_1 \partial \lambda_2}}{\frac{\partial^2 v_0}{\partial \lambda_2^2}}. \tag{17}$$

The aforementioned initial equilibrium BNNT is used as a reference configuration when studying the bending behaviors. The deformation process can be expressed by:

$$\begin{cases} \tilde{x}_1 = x_1 + u_1 \\ \tilde{x}_2 = x_2 + u_2, \\ \tilde{x}_3 = u_3 \end{cases} \tag{18}$$

where $u_1$, $u_2$ and $u_3$ are the relative displacements to its undeformed counterparts along $x_1$, $x_2$ and $x_3$ directions, respectively. Higher-order gradient theory is used to calculate the total potential for the system

$$E = \int_{\Omega} W(\tilde{\mathbf{F}}, \tilde{\mathbf{G}}) \mathrm{d}V - \int_{\partial\Omega} \mathbf{u} \cdot \mathbf{t}_0^P \mathrm{d}S - \int_{\partial\Omega} \nabla_N \mathbf{u} \cdot \mathbf{t}_0^Q \mathrm{d}S, \tag{19}$$

where $\mathbf{t}_0^P$ and $\mathbf{t}_0^Q$ denote the first- and the second-order stress tractions on the domain surface, respectively. The equilibrium configuration of BNNTs under an external load is determined by varying total energy of the system, giving the weak form as:

$$\int_{\Omega} \delta \mathbf{grad}^T \cdot \boldsymbol{\sigma} \mathrm{d}V - \int_{\partial\Omega} \delta \mathbf{u}^T \cdot \mathbf{t}_0^P \mathrm{d}S - \int_{\partial\Omega} (\nabla_N \delta \mathbf{u}) \cdot \mathbf{t}_0^Q \mathrm{d}S = 0, \tag{20}$$

where $\boldsymbol{\sigma} = \frac{\partial v}{\partial \mathbf{grad}}$ with $\mathbf{grad} = [\tilde{\mathbf{F}} \quad \tilde{\mathbf{G}}]$.

The governing equation of bending deformation of BNNTs in equation (20) is solved by our mesh-free computational framework on the basis of moving Kriging interpolation which has been written by Fortran code. Detailed procedure can be referred to our previous work [45].

## 3 Results and discussion

There is still no generally accepted one-atomic material thickness which has troubled scholars for a long time. In a continuum mechanics model, many parameters including cross-sectional area, elastic properties, flexural rigidity and moment of inertia closely rely on the thickness, especially when the tubular radius enters to the nanometer level. However, the academic community has not reached a consensus on the thickness of one-atomic material. Scattered values of thickness exist, which caused different static bending deflections and transverse vibration natural frequency. In many literature studies, the interlayer space is widespreadly used, and the obtained results regarding the static and dynamic behaviors evaluated by classical continuum theories are always biased from the atomic simulations to a greater or lesser degree. Such deviations are generally corrected by introducing the scale parameters to the modified continuum theories.

In this study, the thickness of BNNTs, viewed as rolling up an h-BN sheet into a seamless hollow cylinder, is inherited as that of the h-BN sheet as determined in our previous work [42]. Scale effect can be reflected by elastic constant, which relies on tubular radius and length has been semi-analytically investigated in our recently developed atomistic-continuum multiscale approach [46]. Data listed in Table 1 are the predicted elastic parameters and tubular radii for the three kinds of armchair BNNTs. It clearly demonstrates that the curvature has a slight decreasing effect on the axial Young's modulus while an opposite effect on Poisson's ratio.

Classical EBT is used to analytically predict the bending deflection of BNNTs under lateral load. Numerical results obtained by an atomic-continuum multi-scale approach directly constructed from the "bottom-up" force field with no external introduced parameters, such as Young's modulus, thickness and bending stiffness, are provided for comparison. Plotted in Figure 1 are the schematic diagrams of bending deflection for hollow single-walled BNNTs under transverse load. EBT with two typical constraints, i.e., simply supported and clamped boundary conditions, based on our determined value 0.0906 nm is employed to predict the bending deflection of BNNTs under transverse load, and EBT solutions based on the commonly used interlayer space 0.333 nm are also provided for comparison.

The maximum bending deflection occurs at the midpoint of the beam. Figure 2 demonstrates the relationship between midpoint bending deflections of simply supported 10 nm long (8, 8) and (10, 10) BNNTs obtained by EBT as well as atomistic-continuum multiscale

**Table 1:** Elastic properties of armchair BNNTs

| (*n*, *m*) | *R* (Å) | *E* (TPa) | *M* |
|---|---|---|---|
| (8, 8) | 5.51 | 3.5346 | 0.1798 |
| (10, 10) | 6.90 | 3.5509 | 0.1736 |
| (15, 15) | 10.36 | 3.5671 | 0.1675 |

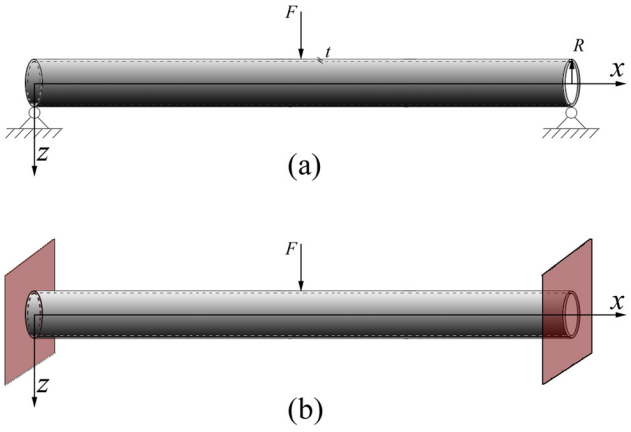


**Figure 1:** Schematic diagram of bending deflection for hollow single-walled BNNTs with simply supported (a) and clamped (b) constraints under transverse load.

approach. The length/diameter ($l/d$) ratios are 9.07 and 7.25, respectively. It clearly reveals that both EBT solutions with the commonly used interlayer space differ from atomistic-continuum simulation results but within limits. This deviation is often corrected by modified continuum theories involving the scale effect parameter. For example, nonlocal elasticity theory has a "stiffness soften" effect (the equivalent nanostructural stiffness decreases when one-atomic material thickness is adopted) on the flexural stiffness of beam [47–49], thus the bending deflections will be enlarged to approach those of atomic simulations. As a matter of fact, the underestimation of the bending deflections is due to the used larger tubular thickness. When we inherit the well-determined thickness of an h-BN sheet, it is found that EBT can quite accurately predict the bending deflection of the atomistic-continuum approach. As compared with the two cases, it is found that the relative deviation of EBT using the interlayer space to the atomistic-continuum approach for BNNTs becomes smaller as tubular radius increases. This is because the moment of inertia becomes insensitive to tubular thickness as the tubular radius increases and thus the flexural rigidity. This phenomenon yields the different scale parameters for specific case studies when the modified theories are used.

For slender beams with larger $l/d$ ratio, EBT is expected to give much more accurate predictions, and the results are given in Figures 3 and 4. Figure 3 plots the force–displacement curves for 12 nm long simply supported (8, 8) and (10, 10) BNNTs with a $l/d$ ratio of 10.89 and 8.70, respectively. Figure 4 shows those of 15 nm long BNNTs with $l/d$ ratios of 13.61 and 10.87, and the maximum extent of EBT results with two material thicknesses are shown as the error bar. Figures 3(a) and 4(a) reveal that EBT with a tubular thickness of 0.0906 nm accurately estimates the results obtained by the atomistic-continuum approach under a small range of concentrated forces, while overestimate them as the force continues to increase with an increasing tendency of deviation. This is mainly due to the geometrical nonlinearity which becomes increasingly severe as the tubular length increases since the bending deflection is a cubic function of tubular

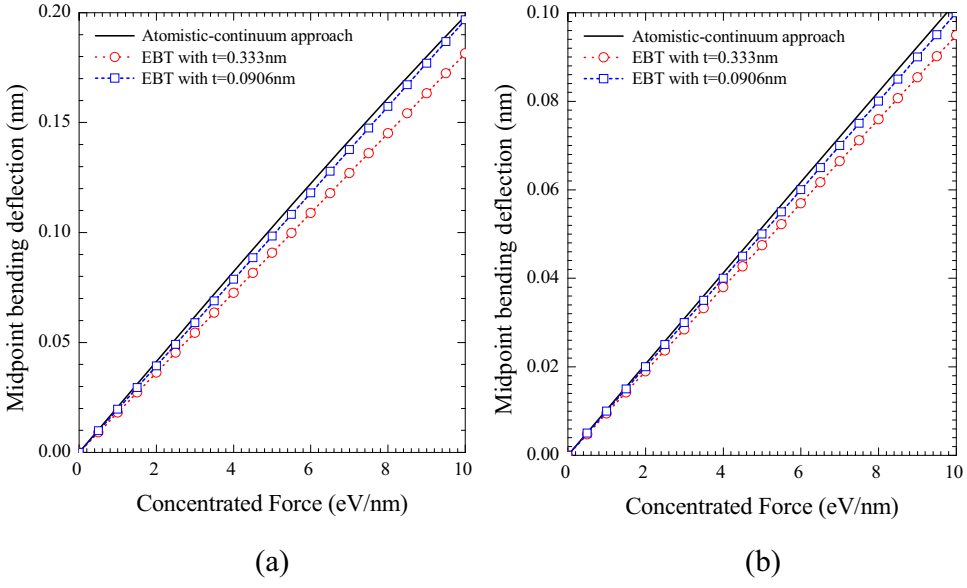


**Figure 2:** The midpoint bending deflection of 10 nm long (8, 8) (a) and (10, 10) (b) BNNTs with simply supported constraint versus external transverse force.

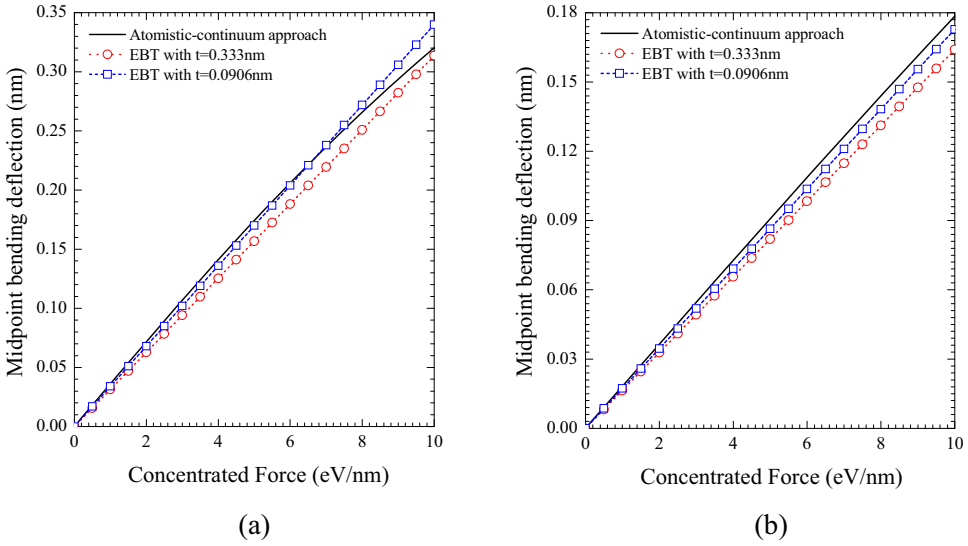


**Figure 3:** The midpoint bending deflection of 12 nm long (8, 8) (a) and (10, 10) (b) BNNTs with simply supported constraint versus external transverse force. A nonlinear relation between transverse load and bending deflection is observed.

length. The EBT results with one-atomic material thickness of BNNTs present smaller errors compared with those with interlayer space, as shown in Figure 4a. Since flexural rigidity is a function of quartic function of the tubular radius, increasing tubular radius yields a rapidly decreasing bending deflection, thus lags behind the nonlinear effect phenomenon as shown in Figures 3(b) and 4(b).

The boundary constraint on the bending behaviors of BNNTs is also investigated. As expressed by equation (7), the bending deflection of beam with clamped constraint is quite less than simply supported one. Figures 5–7 are the force–displacement curves for the midpoint of 10 nm long (8, 8) and (10, 10) clamped BNNTs. As expected, the present tubular thickness also results in a much better agreement than the widely used interlayer space. Besides, the maximum bending deflection is in a smaller range than those simply supported ones because the nonlinear effect does not begin to show up. An unusual observed phenomenon is that EBT solutions with interlayer space tubular thickness seem to give a better prediction of the atomistic-continuum

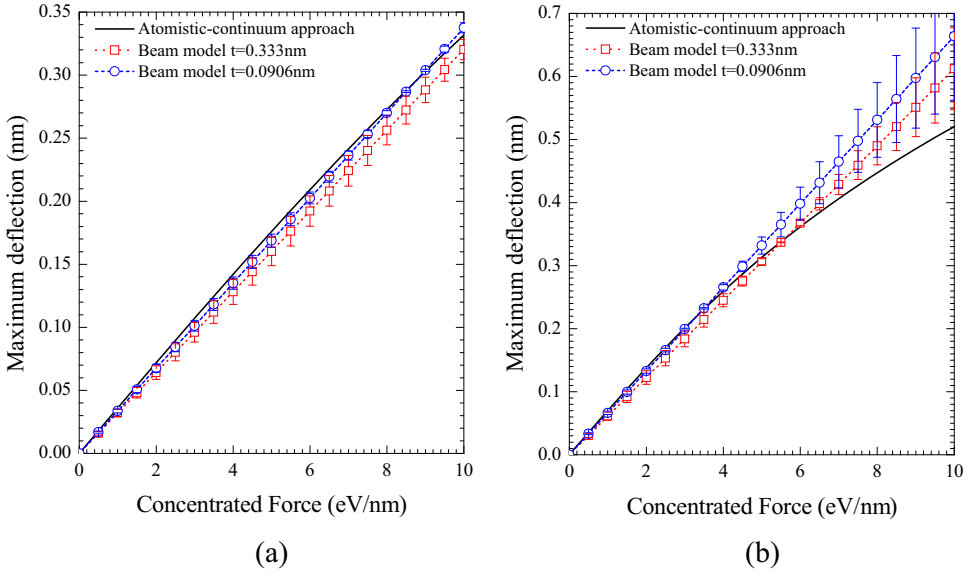


**Figure 4:** The midpoint bending deflection of 15 nm long simply supported (8, 8) (a) and (10,10) (b) BNNTs. A linear relation between the transverse load and bending deflection is observed at the first half, while a clear nonlinear relation is observed at the latter half.

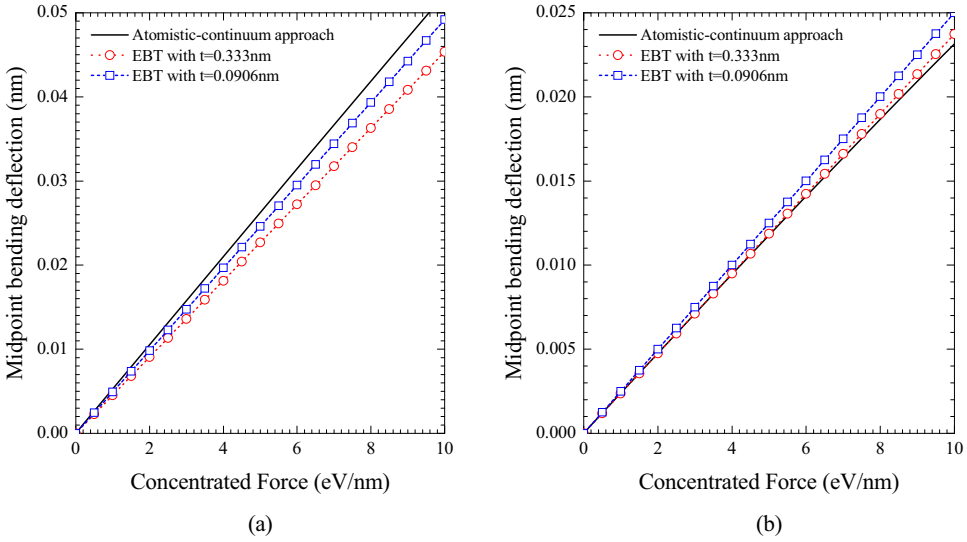


**Figure 5:** The maximum bending deflection of 10 nm long (8, 8) (a) and (10, 10) (b) BNNTs with clamped constraint versus external lateral force.

approach than those with 0.0906 nm tubular thickness for the clamped 10 nm (10, 10) BNNT in Figure 5(b). This resulted from the larger diameter. As the tubular radius increases, the $l/d$ ratio is only 7.25 and the influence of shear deformation becomes more and more important, especially for the strong constraint, which leads to overestimation of bending deflection.

Overall, when the current thickness of 0.0906 nm is adopted, the results predicted by EBT are much more closer to the atomistic-continuum simulation results. What should be noted is that EBT generally has an increasing error when the aspect ratio decreases, which can almost be omitted when the aspect ratio is larger than 10.

## 4 Concluding remarks

In this work, atomistic-continuum multiscale approach and classical Euler–Bernoulli theory are employed to predict the transverse bending deflection behavior of single-walled BNNTs with two typical boundary constraints.

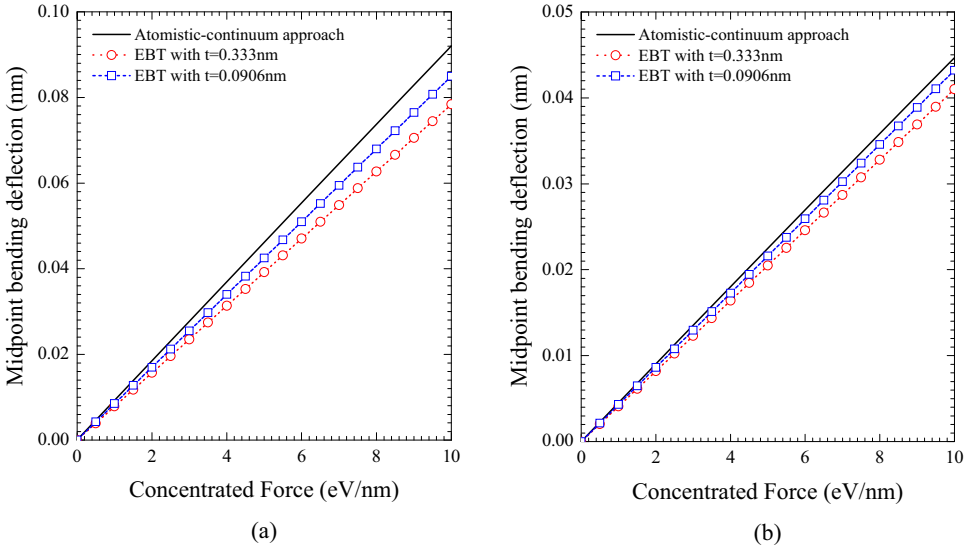


**Figure 6:** The midpoint bending deflection of 12 nm long (8, 8) (a) and (10, 10) (b) BNNTs with clamped constraint versus external lateral force.

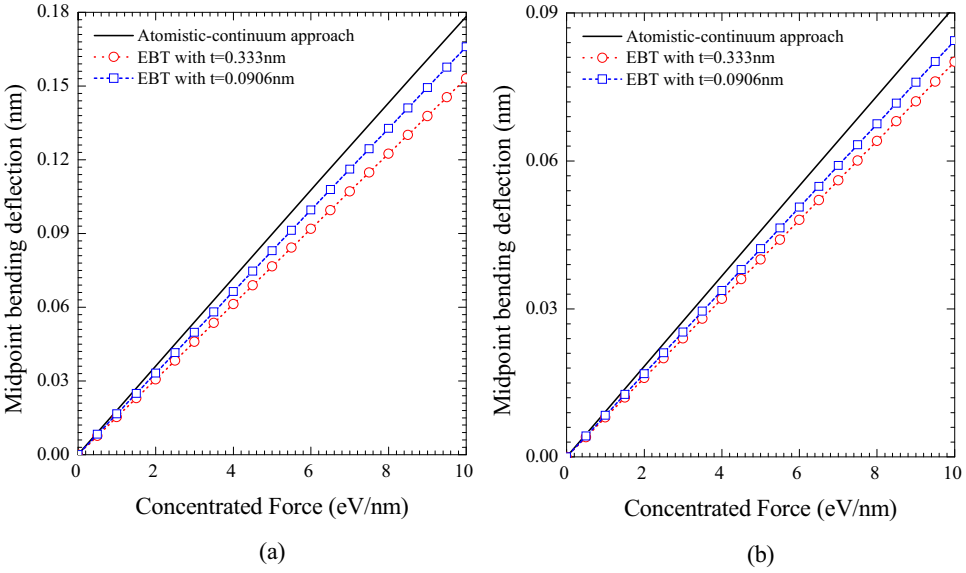


**Figure 7:** The midpoint bending deflection of 10 nm long (8, 8) (a) and (10, 10) (b) BNNTs with clamped constraint versus external transverse force.

Considering two different thicknesses of single-wall BNNTs, the analytical results of the bending deflections are given by the classical Euler–Bernoulli theory. In contrast, numerical results obtained by the atomic-continuum multi-scale approach directly constructed from force field with no external introduced parameters, such as Young's modulus, thickness and bending stiffness, are provided for comparison. With simply supported and clamped constraints, the comparison of calculation results shows that the one-atomic material thickness of BNNTs is a more reasonable value to predict the static behavior of single-walled BNNTs, rather than the interlayer space. As the geometrical nonlinearity increases, EBT with a tubular thickness of 0.0906 nm accurately estimates the results obtained by the atomistic-continuum approach, while overestimates them as the force continues to increase with an increasing tendency of deviation. Comparing the predicted results with two different constraint conditions, it can be found that the results of simply supported constraint are more accurate.

**Acknowledgements:** The work described in this study was fully supported by the research grants from the Natural Science Foundation of China (Grants No. 12072112 and 11702112), National Natural Science Foundation Excellent Youth Cultivation Project (Grant No. 20202ZDB01001) and Natural Science Foundation of Jiangxi Province (Grant No. 20202ACBL214014), and Hong Kong Scholars Program (Project No. XJ2019016).

**Conflict of interest:** The authors declare no conflict of interest regarding the publication of this paper.

## References

[1] Chen H, Zeng S, Chen M, Zhang Y, Li Q. Fabrication and functionalization of carbon nanotube films for high-performance flexible supercapacitors. Carbon. 2015;92:271–96.

[2] Li Z, Xu K, Wei F. Recent progress in photodetectors based on low-dimensional nanomaterials. Nanotechnol Rev. 2018;7(5):393–411.

[3] Dong S, Zhou J, Hui D. A quantitative understanding on the mechanical behaviors of carbon nanotube reinforced nano/ultrafine-grained composites. Int J Mech Sci. 2015;101:29–37.

[4] Lin X, Han Q, Huang J. Effect of defects on the motion of carbon nanotube thermal actuator. Nanotechnol Rev. 2019;8(1):79–89.

[5] Levshov DI, Tran HN, Paillet M, Arenal R, Than XT, Zahab AA, et al. Accurate determination of the chiral indices of individual carbon nanotubes by combining electron diffraction and Resonant Raman spectroscopy. Carbon. 2017;114:141–59.

[6] Ramesh S, Khandelwal S, Rhee KY, Hui D. Synergistic effect of reduced graphene, CNT and metal oxides on cellulose matrix for supercapacitor applications. Compos Part B. 2018;138:45–54.

[7] Bu IYY, Oei SP. Hydrophobic vertically aligned carbon nanotubes on Corning glass for self cleaning applications. Appl Surf Sci. 2010;256(22):6699–704.

[8] Song L, Toth G, Vajtai R, Endo M, Ajayan PM. Fabrication and characterization of single-walled carbon nanotube fiber for electronics applications. Carbon. 2012;50(15):5521–24.

[9] Ventrapragada LK, Creager SE, Rao AM, Podila R. Carbon nanotubes coated paper as current collectors for secondary Li-ion batteries. Nanotechnol Rev. 2019;8(1):18–23.
[10] Lu Y, Liu J, Hou G, Ma J, Wang W, Wei F, et al. From nano to giant? Designing carbon nanotubes for rubber reinforcement and their applications for high performance tires. Compos Sci Technol. 2016;137:94–101.
[11] Hashim H, Salleh MS, Omar MZ. Homogenous dispersion and interfacial bonding of carbon nanotube reinforced with aluminum matrix composite: A review. Rev Adv Mater Sci. 2019;58(1):295–303.
[12] Yu I, Ko J, Kim TW, Lee DS, Kim ND, Bae S, et al. Effect of sorted, homogeneous electronic grade single-walled carbon nanotube on the electromagnetic shielding effectiveness. Carbon. 2020;167:523–9.
[13] Wang T, Lu J, Zhu H, Liu J, Lin X, Liu Y, et al. The electronic properties of chiral carbon nanotubes. Comp Mater Sci. 2017;129:290–4.
[14] Blasé X, Rubio A, Louie SG, Cohen ML. Stability and band gap constancy of boron nitride nanotubes. Europhys Lett. 1994;28(5):335–40.
[15] Ciofani G, Raffa V, Menciassi A, Cuschieri A. Boron nitride nanotubes: An innovative tool for nanomedicine. Nano Today. 2009;4(1):8–10.
[16] Ansari R, Ajori S, Ameri A. Stability characteristics and structural properties of single- and double-walled boron-nitride nanotubes under physical adsorption of Flavin mononucleotide (FMN) in aqueous environment using molecular dynamics simulations. Appl Surf Sci. 2016;366:233–44.
[17] Giannopoulos, Georgios I. On the buckling of hexagonal boron nitride nanoribbons via structural mechanics. Superlattice Microst. 2018;115:1–9.
[18] Ghassemi HM, Yassar RS. On the mechanical behavior of boron nitride nanotubes. Appl Mech Rev. 2010;63(2):0804.
[19] Zhi C, Bando Y, Tang C, Honda S, Kuwahara H, Golberg D. Boron nitride nanotubes/polystyrene composites. J Mater Res. 2006;21(11):2794–800.
[20] Peng Q, Ji W, De S. Mechanical properties of the hexagonal boron nitride monolayer: Ab initio study. Comp Mater Sci. 2012;56:11–7.
[21] Yan JW, Liew KM. Predicting elastic properties of single-walled boron nitride nanotubes and nanocones using an atomistic-continuum approach. Compos Struct. 2015;125:489–98.
[22] Ding Q, Ding N, Liu L, Li N, Wu C. Investigation on mechanical performances of grain boundaries in hexagonal boron nitride sheets. Int J Mech Sci. 2018;149:262–72.
[23] Liang Y, Qin H, Huang J, Huan S, Hui D. Mechanical properties of boron nitride sheet with randomly distribute vacancy defects. Nanotechnol Rev. 2019;8:210–7.
[24] Oh ES. Elastic properties of boron-nitride nanotubes through the continuum lattice approach. Mater Lett. 2010;64(7):859–62.
[25] Ashton TS, Moore AL. Foam-like hierarchical hexagonal boron nitride as a non-traditional thermal conductivity enhancer for polymer-based composite materials. Int J Heat Mass Tran. 2017;115:273–81.
[26] Pan Y, Li L, Yuan X, Guo J, Yang P. Effects of defects on heat conduction of graphene/hexagonal boron nitride heterointerface. Phys Lett A. 2020;384(30):126774.
[27] Ren L, Zeng X, Sun R, Xu J, Wong CH. Spray-assisted assembled spherical boron nitride as fillers for polymers with enhanced thermally conductivity. Chem Eng J. 2019;370:166–75.
[28] Zahedi E, Seif A. Effect of tube radius on the electronic and magnetic properties of finite boron nitride zigzag nanotubes using DFT. Phys E. 2011;44(1):179–85.
[29] Raissi H, Mollania F. Immunosuppressive agent leflunomide: A SWNTs-immobilized dihydroortate dehydrogenase inhibitory effect and computational study of its adsorption properties on zigzag single walled (6,0) carbon and boron nitride nanotubes as controlled drug delivery devices. Eur J Pharm Sci. 2014;56:37–54.
[30] Soltani A, Raz SG, Rezaei VJ, Khalaji AD, Savar M. Ab initio investigation of Al- and Ga-doped single-walled boron nitride nanotubes as ammonia sensor. Appl Surf Sci. 2012;263:619–25.
[31] Yoosefian M, Etminan N, Moghani MZ, Mirzaei S, Abbasi S. The role of boron nitride nanotube as a new chemical sensor and potential reservoir for hydrogen halides environmental pollutants. Superlattice Microst. 2016;98:325–31.
[32] Movlarooy T, Fadradi MA. Adsorption of cyanogen chloride on the surface of boron nitride nanotubes for CNCl sensing. Chem Phys Lett. 2018;700:7–14.
[33] Ahangari MG, Fereidoon A, Mashhadzadeh AH. Interlayer interaction and mechanical properties in multi-layer graphene, boron-nitride, aluminum-nitride and gallium-nitride graphene-like structure: a quantum-mechanical DFT study. Superlattice Microst. 2017;112:30–45.
[34] Girard M, Ehlen A, Shakya A, Bereau T, Olvera M. A highly object-oriented builder for molecular dynamics. Comp Mater Sci. 2019;167:25–33.
[35] Wang H, Guilleminot J, Soize C. Modeling uncertainties in molecular dynamics simulations using a stochastic reduced-order basis. Comput Method Appl M. 2019;354:37–55.
[36] Yang W, Fang C, Wang X. Nonlinear dynamic characteristics of FGCNTs reinforced microbeam with piezoelectric layer based on unifying stress-strain gradient framework. Compos Part B-Eng. 2017;111:372–86.
[37] Karamanli A, Vo TP. Size-dependent behaviour of functionally graded sandwich microbeams based on the modified strain gradient theory. Compos Srtuct. 2020;246:112401.
[38] Karami B, Janghorban M, Rabczuk T. Static analysis of functionally graded anisotropic nanoplates using nonlocal strain gradient theory. Compos Srtuct. 2019;227:111249.
[39] Asemi SR, Farajpour A, Mohammadi M. Nonlinear vibration analysis of piezoelectric nanoelectromechanical resonators based on nonlocal elasticity theory. Compos Struct. 2014;116:703–12.
[40] Zhang Y, Li G, Hui D, Liew KM. Modeling the postbuckling behavior of thermal-resistant ultrathin films attached to glass substrate. Compos Srtuct. 2018;206:279–87.
[41] Zhang Y, Li G, Liew KM. Thermomechanical buckling characteristic of ultrathin films based on nonlocal elasticity theory. Compos Part B-Eng. 2018;153:184–93.
[42] Yan JW, Tong LH, Luo RJ, Gao D. Thickness of monolayer h-BN nanosheet and edge effect on free vibration behaviors. Int J Mech Sci. 2019;164:105163.

[43] Yan JW, Lai SK. Superelasticity and wrinkles controlled by twisting circular graphene. Comput Method Appl M. 2018;338:634–56.
[44] Yan JW, Lai SK, He LH. Nonlinear dynamic behavior of single-layer graphene under uniformly distributed loads. Compos Part B-Eng. 2019;165:473–90.
[45] Yan JW, Liew KM, He LH. Analysis of single-walled carbon nanotubes using the moving Kriging interpolation. Comput Method Appl M. 2012;229–232:56–67.
[46] Yan, JW, Liew KM. Predicting elastic properties of single-walled boron nitride nanotubes and nanocones using an atomistic-continuum approach. Compos Struct. 2015;125:489–98.
[47] Liu JJ, Li C, Fan XL, Tong LH. Transverse free vibration and stability of axially moving nanoplates based on nonlocal elasticity theory. App Math Model. 2017;45:65–84.
[48] Nguyen NT, Hui D, Lee J, Nguyen-Xuan H. An efficient computational approach for size-dependent analysis of functionally graded nanoplates. Comput Method Appl M. 2015;297:191–218.
[49] Li C, Yao LQ, Chen WQ, Li S. Comments on nonlocal effects in nano-cantilever beams. Int J Eng Sci. 2015;87:47–57.